IEICE TRANS. FUNDAMENTALS, VOL.E90–A, NO.10 OCTOBER 2007

PAPER Special Section on Nonlinear Theory and its Applications

An Inhibitory Neural-Network Circuit Exhibiting Noise Shaping with Subthreshold MOS Neuron Circuits

Akira UTAGAWA[†a)], ***Student Member***, **Tetsuya ASAI**[†], **Tetsuya HIROSE**[†], ***and*** **Yoshihito AMEMIYA**[†], ***Members***

SUMMARY We designed subthreshold analog MOS circuits implementing an inhibitory network model that performs noise-shaping pulse-density modulation (PDM) with noisy neural elements, with the aim of developing a possible ultralow-power one-bit analog-to-digital converter. The static and dynamic noises given to the proposed circuits were obtained from device mismatches of current sources (transistors) and externally applied random spike currents, respectively. Through circuit simulations we confirmed that the circuit exhibited noise-shaping properties, and signal-to-noise ratio (SNR) of the network was improved by 7.9 dB compared with that of the uncoupled network as a result of noise shaping.

key words: *neuromorphic analog integrated circuits, pulse density modulation, noise shaping, subthreshold CMOS circuits*

1. Introduction

The purpose of this paper is to explore a possible ultralow-power one-bit analog-to-digital converter (ADC). An one-bit ADC converts analog input signals to digital pulse streams where the analog information is represented in the time domain. This operation is referred to as pulse-density modulation (PDM). A similar operation can be found in spiking neurons [1], e.g., integrate-and-fire neurons (IFNs). The firing rate of the neuron increases as the amount of inputs increases. Hence, the spike trains, e.g., the density of spikes per second, represent analog values consisting of 1-0 digital streams. Therefore an one-bit ADC could theoretically be developed by implementing such a neuron circuit on analog VLSIs. But practically, it is not easy to develop the ADC with a neuron circuit due to the existence of quantization, static and dynamic noises from natural environment as observed in irregular and random firings of biological neurons [2], [3]. The quantization noises can be eliminated by employing a sigma-delta modulator [4], however, eliminating the static noises requires an additional calibration process after the chip fabrication, and eliminating the dynamic noises requires a special isolation device.

In this paper, we explore a possible way to handle both static and dynamic noises in analog integrated circuits by employing neuromorphic architectures. To achieve this, we employ a population model of spiking neurons that exhibits noise shaping [5]. Through numerical and circuit simulations of the network circuit, we demonstrate that the network can improve the system's signal-to-noise ratio (SNR) as a result of effectively using the static and dynamic noises.

Manuscript received December 11, 2006.
Manuscript revised April 6, 2007.
Final manuscript received May 22, 2007.

[†]The authors are with the Graduate School of Information Science and Technology, Hokkaido University, Sapporo-shi, 060-0814 Japan.
a) E-mail: utagawa@sapiens-ei.eng.hokudai.ac.jp

DOI: 10.1093/ietfec/e90–a.10.2108

2. Brief Review of Mar's Neural Network Model

Figure 1(a) illustrates a simple pulse-density modulator for one-bit AD conversion. Analog input signal (voltage or current) is given to a modulator (white circle in the figure), and the modulator produces output (voltage or current) pulses whose frequency is proportional to the analog input. A similar function is performed with spiking neurons, e.g., integrate-and-fire neurons (IFN), as shown in Fig. 1(b). An IFN (white circle in the figure) accepts excitatory and inhibitory presynaptic analog currents (EPSC and IPSC) through excitatory and inhibitory synaptic weights (α and K), and produces output (voltage or current) pulses whose frequency is proportional to $\alpha\times$EPSC $-$ $K\times$IPSC. Mar et al. proposed an inhibitory neural network with noisy IFNs, where the membrane potentials of the IFNs were reset to random values, and random synaptic weights between the

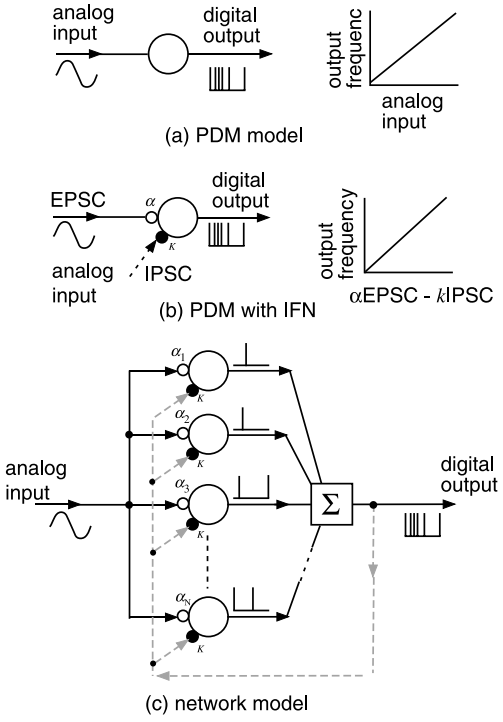

Fig. 1 PDM with Mar's inhibitory neural network model.

IFNs and the external analog inputs were employed [5]. They demonstrated that the noisy inhibitory network could exhibit noise-shaping properties as observed in conventional sigma-delta type ADCs. Figure 1(c) shows a schematic of their network model. The network consists of N IFNs (white big circles) and a global inhibitor($\sum$) (white square). An analog input is commonly given to the IFNs, while the digital output is represented by the sum of spike outputs of all the IFNs. In the figure, α_i represents a distributed (random) input weight between the common analog input and the i-th IFN. When an IFN fires, the membrane potential is reset to random values. A global inhibitor ($\sum$) accepts the sum of outputs of all the IFNs, and inhibits all the IFNs. This model is all-to-all inhibitory network having $O(N^2)$ wiring complexity for N IFNs, however, since the synaptic weights were uniform in the network, we here employ a network of $O(N)$ wiring complexity, aiming at the compact hardware implementation [6], [7].

The membrane potential of the i-th IFN (V_i) is defined by

$$\frac{dV_i}{dt} = -\frac{V_i}{\tau_{\mathrm{m}}} - \sum_{j=1}^{N} \sum_{m} K\gamma(t - t_j^m) + \alpha_i I(t), \tag{1}$$

where τ_m represents the time constant, K the common synaptic weight between IFNs, $I(t)$ the common analog input, α_i the random synaptic weight between the i-th neuron and the common analog input, $t_j^m (m = 1, 2, 3 \cdots)$ the set of firing times of the j-th neuron, and

$$\gamma(t') = \exp\left(-\frac{t'}{\tau_s}\right) \quad (t' > 0), \tag{2}$$

where τ_s is the time constant. Each IFN fires when V_i exceeds a given threshold voltage (V_{th}), and the membrane potential (V_i) is reset to random values between 0 and $0.75V_{\mathrm{th}}$ [5]. It should be noted that this type of inhibitory neural networks exhibit winner-takes-all [8], [9] or winners-share-all [10], [11] type neural competition depending on the strength of inhibitory connection, e.g., it is K in the Mar's model. According to the Mar's theory [5], the degree of noise shaping is proportional to $(MK)^2$, where M represents the number of survived neurons among N neurons. Therefore, we have to choose an appropriate K for $M \rightarrow N$ for winners-share-all type neural competition.

Mar et al. demonstrated that his network model with $N = 50$ exhibited noise-shaping PDM where the amount of the common analog input was converted to pulse densities of the sum of spikes of all the IFNs. Our purpose here is to utilize this function produced by the neuromorphic architecture because neural networks may provide a possible way to develop ultralow-power LSIs by employing subthreshold CMOS devices. However, for practical hardware implementation, N must be small. In this paper, we employ three neurons ($N = 3$) and choose an appropriate K to keep $(MK)^2$ high.

Remember that static noises are embedded in synaptic weights α_i between the common analog inputs and IFNs, whereas dynamic noises are given by resetting each IFN's membrane potential to random values after the firing, in the Mar's network model. To evaluate the effect of these noises in our small-scale network, we consider the network operation under the following three conditions; (i) no noise is given, (ii) only static noises are given, (iii) both static and dynamic noises are given. The simulation results are shown in Fig. 2. In the Mar's original network, $(MK)^2$ was $(50 \times 50)^2 = 2500^2$, whereas we here set $M(= N)$ at 3 and $K = 1000$, which results in $(MK)^2 = 3000^2$. Also to keep the same average firing frequency(≈ 1 kHz) as the original network, we set $I(t)$ at a constant value (1100). Figures 2(a), (b), and (c) represent the inter-spike-interval (ISI) histogram[†], the auto-correlation function (ACF) $\alpha(\tau)$[††], and the power spectrum density (PSD), respectively, when no noises were given to the network, i.e., uniform α_i and uniform reset values were assumed. In this case, we observed three peaks in the ISI histogram (Fig. 2(a)), which results from phase-locked oscillation with a certain phase difference among the IFNs. This implies that, to obtain effective PDM functions by the population of IFNs, we have to set a precisely determined initial condition for each neuron to eliminate this phase difference. In Fig. 2(b), a strong correlation at time shift $\tau = 3$ ms, which is the inverse value of the intrinsic firing frequency (333 Hz) of all the IFNs, was observed. Figure 2(c) shows the PSD of output spikes ('outputs' in Fig. 1(c)) of the network. The power had a peak (upper arrow in the figure) at the IFN's intrinsic firing frequency (333 Hz). As in [12], [13], noise reduction below the intrinsic firing frequency was caused by refractoriness of the individual neuron.

When a static noise was applied (nonuniform α_i was applied), the ISI histogram had a smoother distribution (Fig. 2(d)) as compared to severely localized distributions in Fig. 2(a). In this case, the static noise broke up the phase-locked oscillation and thus normalized the clustering of ISIs. However, a small crest around 1.6 ms was still observed in the histogram, which results from complex interactions among the IFNs and their inhibitory coupling. The ACF is shown in Fig. 2(e). Each IFN has different firing frequency based on nonuniform α_i. When a collective firing frequency is set to 1 kHz with $\alpha_i = 1.0$, 1.1 and 1.2, the IFN's individual firing frequencies are given by 300 Hz, 333 Hz, and 366 Hz, respectively. The upper arrows in Fig. 2(e) indicate inverse values of the intrinsic firing frequencies above. The peaks of the correlation values were shifted toward left and right from the intrinsic firing frequencies because the inhibitory effect spread out the ISIs, whereas it filled up the gaps of the ISIs. The power level below the intrinsic firing frequencies (300 Hz, 333 Hz, and 366 Hz) was increased by about 10 times (Fig. 2(f)) as compared to Fig. 2(c), but the power level around the firing frequencies and above the collective firing frequency (1 kHz) were decreased.

[†]The trial duration was 10.6 s and a bin width was 0.1 ms.

[††]$\alpha(\tau) = \langle X(t')X(t' - \tau)\rangle$, where $X(t)$ is the summed output of Mar's network. The ACF was calculated with time shifts $\tau < 5$ ms using a sampling interval of 0.1 ms.

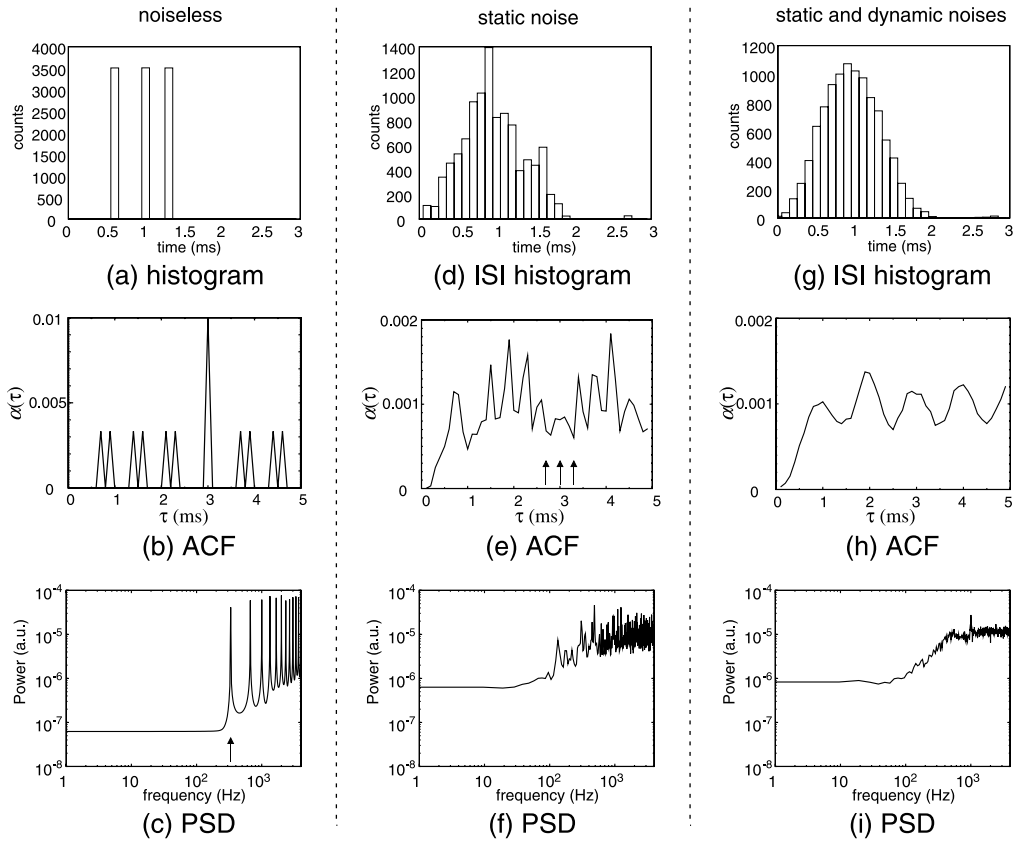

Fig. 2 Simulation results of Mar's inhibitory neural network model.

When both static and dynamic noises are given, i.e., nonuniform α_i and random reset were assumed, the ISI histogram had a Gaussian-like distribution, as shown in Fig. 2(g). Phase randomization caused from the dynamic noise disfavored the oscillation of the IFNs, which averaged the ISIs. The ACF shown in Fig. 2(h) displays oscillations with a period of approximately 1 ms, which indicates that a collective PDM function is obtained with this inhibitory network. Figure 2(i) shows the PSD of this network. The power level was smoothly decreased around the IFN's intrinsic firing frequency and the collective firing frequency (1 kHz), as compared to Fig. 2(f).

Note that the function (one-bit noise-shaping PDM) of the network is the same as conventional delta-sigma ADCs, however, the operational principles of the model are completely different from those of delta-sigma ADCs. Higher order noise shaping in conventional delta-sigma ADCs can be achieved by connecting first-order delta-sigma modulators 'serially' (see, e.g., [4]). On the other hand, according to [5], higher order noise shaping in inhibitory neural networks shown in Fig. 1(c) is achieved by adding integrate-and fire neurons to the network in 'parallel' (increasing the number of neurons).

3. Subthreshold CMOS Neuron Circuit for Implementing Mar's Inhibitory Neural Network

We implement the Mar's noisy IFN using a subthreshold CMOS neuron circuit which has been proposed by Asai et al. [14]. All the MOS transistors in the circuit are operating in their subthreshold region, which ensures ultralow-power consumption as a whole. Therefore, it is suitable to achieve our purpose.

Figure 3 shows schematic of the neuron circuit where C_1 and C_2 represent the capacitance, $V_{\mathrm{m},i}$ the membrane potential of the i-th neuron circuit, U_i the refractory potential, I_i the external input current, $I_{\mathrm{out},i}$ the quantized (spike) output current, I_{ref} the reference current for the quantization and refraction, $I_{\mathrm{d},i}$ the external fluctuation (dynamic noise), and $V_{\mathrm{I},i}$ the inhibitory input. When all the transistors are operating in their subthreshold region [15], the node equations of the circuit are given by

$$C_1 \frac{dV_{\mathrm{m},i}}{dt} = I_i - I_0 e^{\kappa U_i/V_{\mathrm{t}}} + I_{\mathrm{d},i} - I_0 e^{\kappa V_{\mathrm{I},i}/V_t}, \tag{3}$$

$$C_2 \frac{dU_i}{dt} = I_0 e^{\kappa V_{\mathrm{m},i}/V_t} - I_{\mathrm{ref}} + I_{\mathrm{d},i}, \tag{4}$$

where I_0 is the fabrication parameter, κ the effectiveness of the gate potential, V_{t} the temperature dependent term.

Although the circuit's dynamics have been analyzed in

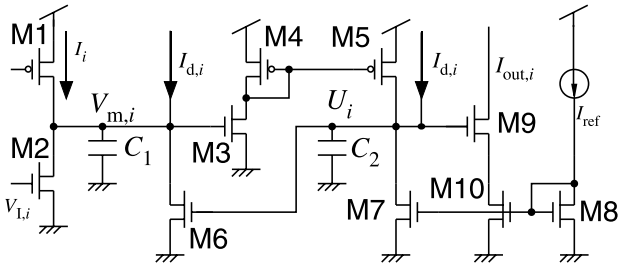

Fig. 3 Subthreshold neuron circuit.

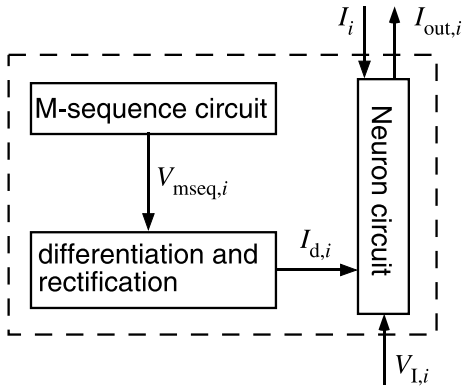

Fig. 4 Block diagram of our noisy neuron circuit consisting of subthreshold neuron circuit, M-sequence circuit for dynamic noise generation and circuit for differentiating and rectifying output of M-sequence circuit.

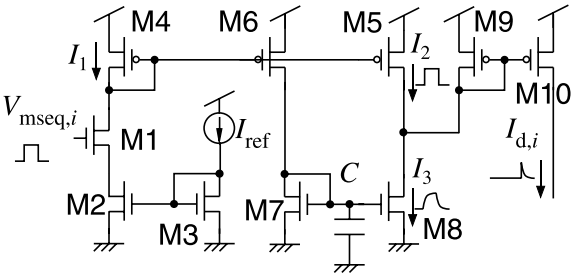

Fig. 5 CMOS circuit for differentiating and rectifying output of M-sequence circuit.

[14], we here describe the operation briefly. The membrane potential ($V_{m,i}$) is increased (or decreased) by charging (or discharging) C_1 through M1 (or M2). M1 acts as an excitatory synapse and accepts external analog input, whereas M2 acts as an inhibitory synapse and accepts an output of a global inhibitor. As $V_{m,i}$ increases, a drain-source current of M3 increases exponentially. The current is copied to node U_i by a current mirror (M4 and M5) and charges C_2, which result in the increase of U_i. If U_i exceeds the threshold voltage of M6, node $V_{m,i}$ is shunted by M6. We define that the time at which $V_{m,i}$ is shunted is the time at which the neuron circuit fires. Since U_i is discharged by a current mirror (M7 and M8), the refractory period, where $V_{m,i}$ cannot increase (the circuit cannot fire) even if excitatory input current I_i were given, is inversely proportional to the amount of reference current I_{ref}. Since M9 accepts U_i, I_{out} is increased when the neuron circuit fires (the shunting current of M6 is increased). Note that the maximum value of I_{out} is regulated by a current mirror (M8 and M10) with reference current I_{ref}.

An external (analog) input is given to the neuron circuit through an excitatory synapse (M1). To embed static noisy coefficient α_i in the i-th IFN of Mar's network into the neuron circuit, we set different dimensions (width/length) of M1 for each neuron circuit only for the simulation use. This size difference is naturally embedded on analog integrated circuits in the fabrication. Note that α_i is proportional to the dimension of M1 of the i-th neuron circuit. On the other hand, dynamic noises are embedded in a different way. In the Mar's network, the dynamic noise was given by resetting the membrane potential to random analog values after the firing. Since producing random analog values is not easy on analog integrated circuits with a compact construction, we apply random current pulses ($I_{d,i}$), whose ISIs obey the Poisson distribution, to nodes $V_{m,i}$ and U_i, instead of setting the source voltage of M6 at time-variant random values. The oscillation phase of Mar's network is increased by resetting the membrane potential, whereas that of the proposed circuit is increased by the current pulses ($I_{d,i}$). Therefore, applying random current pulses to nodes $V_{m,i}$ and U_i is qualitatively the same as the random reset in Mar's original network.

Figure 4 illustrates the construction of the i-th "noisy" neuron circuit that consists of a conventional M-sequence circuit for generating 1-0 digital random streams $V_{mseq,i}$, a circuit that differentiates $V_{mseq,i}$ and produces random current streams $I_{d,i}$ (= 0 or I_{ref}) by rectifying the differentiated voltage, and a neuron circuit shown in Fig. 3. We employ a 8-bit M-sequence circuit with conventional shift registers and an XOR circuit. Figure 5 shows a circuit for the differentiation and rectification. In the circuit, M1 accepts the output of the M-sequence circuit ($V_{mseq,i}$). Since the current of M1 is regulated by a current mirror (M2 and M3) and reference current I_{ref}, I_1 is zero (or I_{ref}) when $V_{mseq,i}$ is logical "0" (or "1"). This current (I_1) is mirrored to I_2 by a current mirror (M4 and M5), and is also mirrored to the capacitance node (C) by a current mirror (M4 and M6). Since capacitor C is added to the common gate of a current mirror (M7 and M8), I_1 is mirrored to I_3 with a time delay. Therefore, $I_2 - I_3$ corresponds to the temporal derivative of I_1. Since a current mirror (M9 and M10) can copy $I_2 - I_3$ only when $I_2 < I_3$ (M9 and M10 rectify $I_2 - I_3$), the output of this circuit ($I_{d,i}$) becomes zero on the rising edge of $V_{mseq,i}$, but becomes nonzero current on the falling edge.

Figure 6 shows the schematic of the network circuit consisting of the noisy neuron circuits and additional MOS circuits (M1, M2 and M3) implementing the global inhibitor shown in Fig. 1(c). Current outputs of noisy neuron circuits ($I_{out,i}$) are summed by M1. The summed current is mirrored by a current mirror (M1 and M2) with a mirror rate of 1:K'. Therefore, the output current (i_{out}) is given by $K' \sum_{i=1}^{3} I_{out,i}$. Since M3 in Fig. 6 and M2 in Fig. 3 forms a current mirror, neuron circuits' membrane potentials ($V_{m,i}$ for all i) are de-

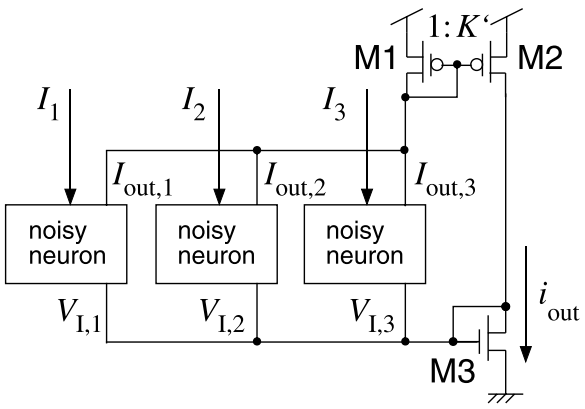

Fig. 6 Network circuit consisting of three noisy neuron circuits and additional circuits (M1, M2 and M3) acting as global inhibitor.

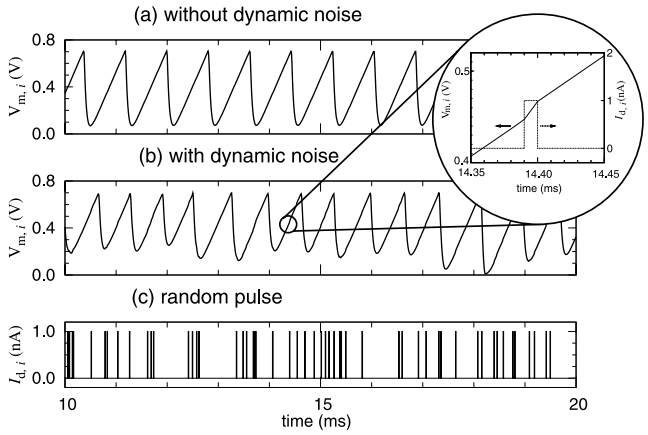

Fig. 7 Simulation results of neuron circuit; (a) time course of membrane potential of neuron circuit without static and dynamic noises; (b) time course of membrane potential of "noisy" neuron circuit with dynamic noise; (c) random pulses given to neuron circuit.

creased when i_{out} is increased, which results in the global inhibition of all the neuron circuits.

4. Simulation Results

In the following circuit simulations, we assumed 1.5-μm CMOS process (MOSIS, Vendor: AMIS). First, we simulated the neuron circuit shown in Fig. 3 to examine the effect of the random current pulses on the circuit as dynamic noises. We assumed that MOS transistors have the same dimension of $W/L = 1.6\,\mu\text{m}/4\,\mu\text{m}$, except for MOS transistors in current mirrors ($W/L = 16\,\mu\text{m}/4\,\mu\text{m}$). The external analog input current (I_i) and the reference current (I_{ref}) were set at 1 nA. The capacitances (C_1 and C_2) were set at 1 pF, and the inhibitory input voltage ($V_{\text{I},i}$) was set at zero. The random current pulses $I_{\text{d},i}$ obeying the Poisson distribution (the mean and variation $\lambda = 5000$) were generated with the amplitude of 1 nA and the pulse width of 10 μs. Figure 7 shows the simulation results of time course of membrane potentials of noiseless ($I_{\text{d},i} = 0$) and noisy ($I_{\text{d},i} \neq 0$) neurons. In Fig. 7(a), we observed periodic oscillation of $V_{\text{m},i}$, whereas nonperiodic oscillation was observed in Fig. 7(b) because the phase was randomly increased by the random current pulses ($I_{\text{d},i}$) shown in Fig. 7(c). Since the neuron circuit produces spike outputs ($I_{\text{out},i}$) when $V_{\text{m},i}$ is suddenly decreased, the operation shown in Fig. 7(b) is equivalent to randomly resetting the membrane potential after the neuron's firing.

As introduced in Sect. 2, all the neuron circuits should survive as a result of neural competition in the inhibitory neural network. Since the number of survivors is decreased (or increased) when the inhibitory connection strength (K) is increased (or decreased), we have to choose an appropriate K for our network circuit through circuit simulations. Normalizing Eq. (3) and comparing it with Eq. (1), we obtain $K = K' I_{\text{ref}}/C_1$ (I_{ref}/C_1 was set at 10^3 in our simulation), which is consistent with K values (10^3) used in Sect. 2. In the simulation, we assumed $N = 3$ and $(\alpha_1, \alpha_2, \alpha_3) = (1, 1.1, 1.2)$ by modifying the ratio of width of transistors M1 in Fig. 3, which results in $(I_1, I_2, I_3) = (1, 1.1, 1.2)$ nA

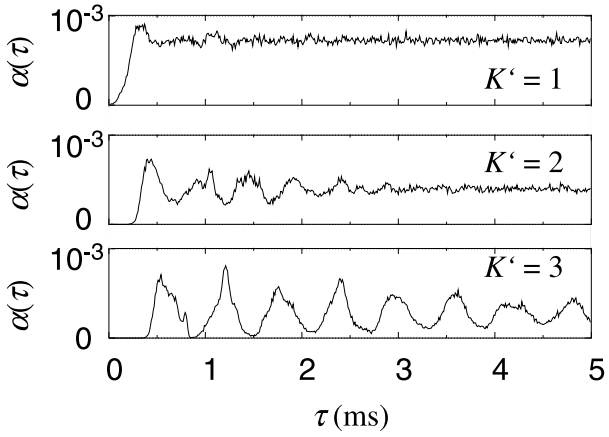

Fig. 8 Auto correlation functions of output of network circuit for $K' = 1$, 2 and 3.

in Fig. 6[†]. We also applied random current pulses $I_{\text{d},i}$ obeying the same Poisson distribution as in the simulations of Fig. 7(b). Through circuit simulations of the network circuit, we found that all the neurons survived when $K' \leq 3$. When $3 < K' < 6$, the membrane potential of a neuron receiving the minimum input current (I_1) was not increased because the amount of the shunting current was larger than that of I_1. When $K' \geq 6$, only one neuron that received the maximum input current (I_3) was survived. To find an appropriate K' that is 3 or less, we calculated ACFs of quantized i_{out} [$\equiv V(t)$] where i_{out} was quantized to 0 (or 1) when i_{out} is smaller (or larger) than 0.8 nA, for $K' = 1$,

[†]Neuron circuit's natural frequency would have an undesirable variation. In our simulations, such variations were simply converged into variations of channel width of M1 ($\sim I_i$) in Fig. 3, instead of considering variations of all transistors in a neuron circuit. As a demonstration, we assumed that the width of M1s were slightly distributed and the resulting drain-to-source current (I_is) were set at $(I_1, I_2, I_3) = (1, 1.1, 1.2)$ nA. These variations (in M1) correspond to variations of input weights (α_i in Fig. 1(c)) which are necessary for obtaining the network's noise shaping properties.

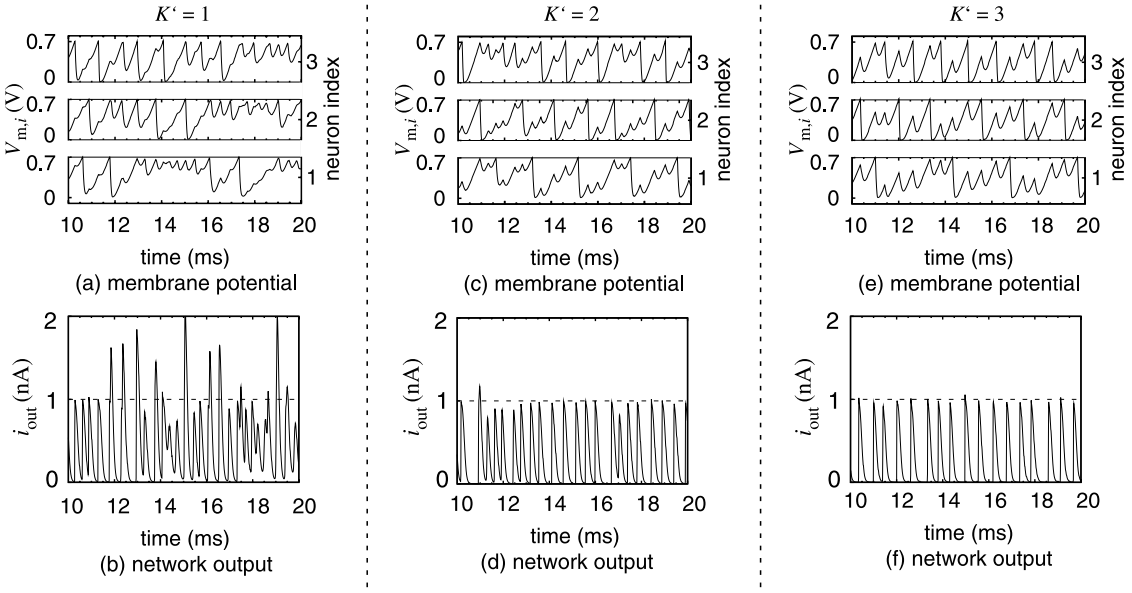

Fig. 9 Time courses of membrane potentials $V_{m,i}$ (i =1, 2 and 3) and network output i_{out} when inhibitory connection strength $K' = 1$, 2 and 3.

2 and 3. Figure 8 shows the results of the ACFs where $\alpha(\tau) = \langle V(t')V(t'-\tau)\rangle$. As K' increased, apparent correlation peaks were appeared, as in Mar's original simulations. Figure 9 shows time courses of membrane potentials $V_{m,i}$ (i =1, 2 and 3) and network output i_{out} when $K' = 1$, 2 and 3. When $K' = 1$, all the neuron circuits survived, as shown in Fig. 9(a), and i_{out} exhibited nonperiodic oscillation (Fig. 9(b)). Since simultaneous firings were happened merely, i_{out} exceeded the regulated current I_{ref} (= 1 nA). When $K' = 2$, the simultaneous firings were drastically reduced, but ISIs of i_{out} were still incoherent, as shown in Figs. 9(c) and (d). When $K' = 3$, all the neuron circuits still survived (Fig. 9(e)). Simultaneous firings were perfectly removed as well as ISIs of i_{out} were almost uniform (Fig. 9(f)), which implies that noises in i_{out} were significantly removed when K' (≤ 3) is increased. Therefore we here fix K' at 3 for our network where i) all the three neurons survive, ii) the ACF has the same characteristics as Mar's one, and iii) the output has uniform ISIs of i_{out} without simultaneous firings.

Figure 10 compares the network circuit operations when $K' = 0$ (uncoupled) and $K' = 3$ (coupled). When $K' = 0$ (Fig. 10(a)), i_{out} exhibited nonperiodic oscillations. Noisy neuron circuits fired incoherently (See raster plots in the figure. +, × and ∗ represent the firing events of the first, the second and the third neuron circuits, respectively.). The resulting ISIs of output spike trains were random. On the other hand, when $K' = 3$, i_{out} exhibited almost periodic oscillations (Fig. 10(b)). The raster plots in the figure show significant differences between firing frequencies of noisy neuron circuits as compared to raster plots in Fig. 10(a). The resulting ISIs of output spike trains were almost uniform, as expected.

Figure 11 shows ISI histograms of the uncoupled ($K' = 0$) and coupled ($K' = 3$) network circuits where 1500 firing

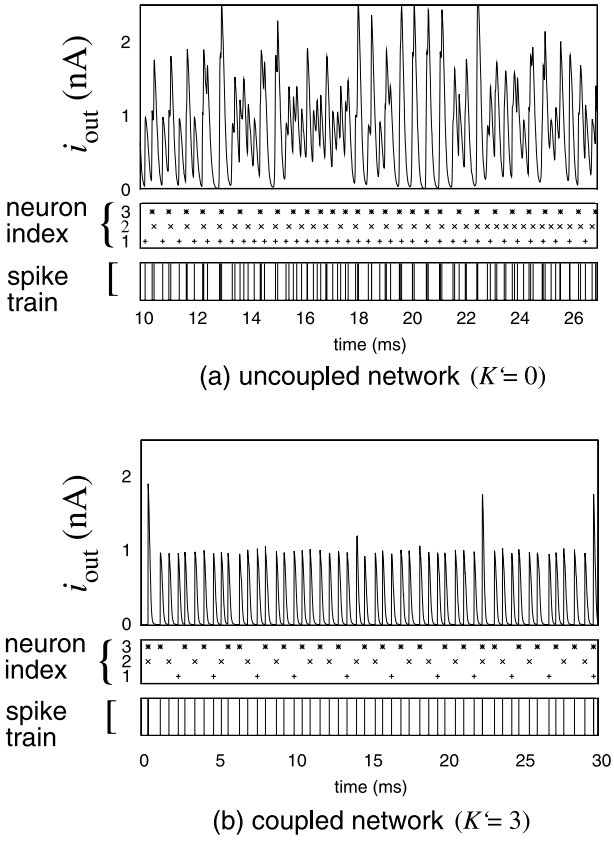

Fig. 10 Comparison of network circuit operations when $K' = 0$ (uncoupled network) and $K' = 3$ (coupled network).

events were gathered with $\Delta = 0.01$ ms. When $K' = 0$, we observed a Poisson-type distribution of ISIs (solid line in Fig. 11) because each neuron circuit was driven by indepen-

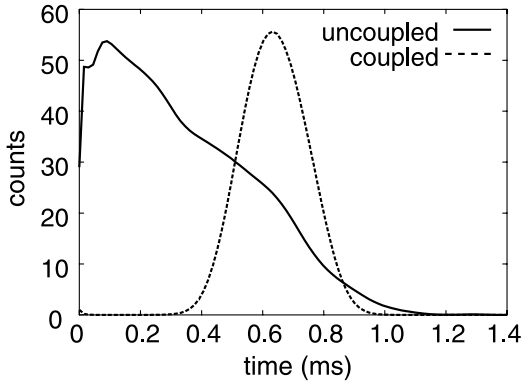

Fig. 11 ISI histograms of uncoupled ($K' = 0$) and coupled ($K' = 3$) networks.

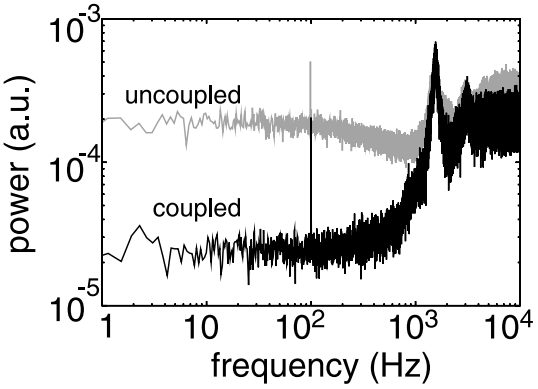

Fig. 12 Power spectra of uncoupled ($K' = 0$) and coupled ($K' = 3$) networks.

dent noise sources and was thus fired incoherently. When $K' = 3$, a Gaussian-type distribution was observed (dashed line in Fig. 11). Once a neuron circuit receiving the maximum external input fires, the network is globally inhibited. After this firing, the neuron circuit operates in its refractory state. Therefore, ISIs of this neuron are increased as compared to uncoupled case. Also, the neuron circuit cannot fire when the other neuron circuit, which receives smaller input than the maximum input, fires. Therefore, ISIs of output spike trains follow ISIs of a neuron receiving the maximum input, and the ISIs are averaged over whole neurons' firing events.

Figure 12 shows the PSD of the coupled ($K' = 3$) and uncoupled ($K' = 0$) networks with sinusoidal inputs ($I_i = I_0 + A\sin(2\pi ft)$, $I_0 = 1$ nA, $A = 50$ pA, $f = 100$ Hz) where 16 trials with different sets of initial values in M-sequence circuits were averaged with a square window function. The measured SNR of the uncoupled network was 10.2 dB, while that of the coupled one was 18.1 dB, which indicated that the noise level of the coupled network was less than one tenth of that of uncoupled network below the cutoff frequency ($< 10^3$ Hz). The external random current pulse obeying the Poisson distribution is theoretically anti-correlated noise. The change in ISI distributions from the Poisson type to Gaussian type in Fig. 11 implies that the amount of noises were decreased by the effect of the global inhibition. As observed in raster plots in Fig. 10(b), individual neurons fired irregularly and thus seemed not to contribute to the signal transmission between the analog input and the digital (spike) output. Moreover, since the firing order of the neurons were also random, they seemed to fire incoherently. However, the resulting output, the sum of firing events of neurons shown in the bottom of Fig. 10(b), were almost periodic. This mechanism is appeared on the resulting PSD (Fig. 12) as the suppression of noises, which implies that the coupled network has an immunity from both static and dynamic noises as compared to the uncoupled network which strongly depends on the noise characteristics of individual neurons.

We roughly estimated power consumption of the proposed circuit. Since the neuron circuit shown in Fig. 3 was biased by 5 V and $O(10^{-9})$ A, the power consumption per a neuron would be in the order of nW (nano-Watt). The associated circuits (M-sequence and 'differentiation and rectification' circuits) shown in Fig. 4 consumed the same order of power as the neuron circuit. Because we employed 3 neuron circuits (Fig. 6) and a global inhibitor (M1 to M3 in the figure), the total power consumption would be several tens to hundreds of nano-Watts. On the other hand, according to the latest data presented in [16], typical one-bit ADCs consumed several micro-Watts to several hundreds of micro-Watts, which indicates that our circuit would be a possible candidate for feature ultralow-power ADCs.

5. Conclusion

We investigated a possible way to develop an one-bit analog-to-digital converter in a noisy environment. We proposed a network circuit inspired by neuromorphic architectures to subtly utilize static and dynamic noise in VLSIs. We employed a population model of spiking neurons [5]. This model has a network using inhibitory coupling that exhibits noise shaping. We implemented this model with subthreshold MOS circuits to actively employ noise. The static and dynamic noise applied to the circuit for noise shaping was obtained from device mismatches of current sources and externally applied random (Poisson) spikes, respectively. A coupled network produced a Gaussian-like distribution of inter-spike intervals (ISIs), while an uncoupled one had a broad distribution of ISIs. Through circuit simulations we confirmed that the signal-to-noise ratio (SNR) of a coupled network was improved by 7.9 dB compared with that of an uncoupled one as a result of noise shaping.

References

[1] M. Hovin, D. Wisland, Y. Berg, J.T. Marienborg, and T.S. Lande, "Delta-sigma modulation in single neurons," Proc. 2002 IEEE International Symposium on Circuits and Systems, vol.5, pp.617–620, 2002.

[2] M.N. Shalden and W.T. Newsome, "The variable discharge of cortical neurons: Implications for connectivity computation, and information coding," J. Neurosci., vol.18, pp.3870–3896, 1998.

[3] W.R. Softky and C. Koch, "The highly irregular firing of cortical cells is inconsistent with temporal integration of random EPSPs," J. Neurosci., vol.14, pp.334–350, 1993.
[4] S.R. Norsworthy, R. Schreier, and G.C. Temes, ed., Delta-Sigma Data Converters, IEEE Press, Piscataway, NJ, 1997.
[5] D.J. Mar, C.C. Chow, W. Gerstner, R.W. Adams, and J.J. Collins, "Noise shaping in populations of coupled model neurons," Neurobiology, 96, pp.10450–10455, 1999.
[6] T. Asai, T. Fukai, and S. Tanaka, "A subthreshold MOS circuit for the Lotka-Volterra neural network producing the winners-share-all solutions," Neural Netw., vol.12, no.2, pp.211–216, 1999.
[7] T. Asai, M. Ohtani, and H. Yonezu, "Analog integrated circuits for the Lotka-Volterra competitive neural networks," IEEE Trans. Neural Netw., vol.10, no.5, pp.1222–1231, 1999.
[8] S. Kaski and T. Kohonen, "Winner-take-all networks for physiological models of competitive learning," Neural Netw., vol.7, no.6-7, pp.973–984, 1994.
[9] J.G. Taylor and F.N. Alavi, "A global competitive neural network," Biol. Cybern., vol.72, pp.233–248, 1995.
[10] T. Fukai and S. Tanaka, "A simple neural network exhibiting selective activation of neuronal ensembles: From winner-take-all to winners-share-all," Neural Comput., vol.9, pp.77–97, 1997.
[11] W.J. Wolfe, D. Mathis, C. Anderson, J. Rothman, M. Gottler, G. Brady, R. Walker, G. Duane, and G. Alaghband, "*K*-winner networks," IEEE Trans. Neural Netw., vol.2, no.2, pp.310–315, 1991.
[12] B.W. Edwards and G.H. Wakefield, "The spectral shaping of neural discharges by refractory effects," J. Acoust. Soc. Am., vol.93, no.6, pp.3353–3364, 1993.
[13] M. Spiridon, C.C. Chow, and W. Gerstner, ed., "Frequency spectrum of coupled stochastic neurons with refractorinness," Proc. ICANN'98, pp.337–342, 1998.
[14] T. Asai, Y. Kanazawa, and Y. Amemiya, "A subthreshold MOS neuron circuit based on the Volterra system," IEEE Trans. Neural Netw., vol.14, no.5, pp.1308–1312, 2003.
[15] E.A. Vittoz, "Micropower techniques," in Design of MOS VLSI Circuits for Telecommunications, ed. Y. Tsividis and P. Antognetti, pp.104–144, Prentice-Hall, Englewood Cliffs, NJ, 1985.
[16] H.Y. Yang and R. Sarpeshkar, "A bio-inspired ultra-energy-efficient analog-to-digital converter for biomedical applications," IEEE Trans. Circuits Syst. I, vol.53, no.11, pp.2349–2356, 2006.

Akira Utagawa received the B.S. degree in electrical engineering from Hokkaido University, Sapporo, Japan, in 2006. He is currently working toward the M.E., degree in the Department of Electrical Engineering, Hokkaido University, Sapporo, Japan. His current research interests are in low-power analog CMOS circuits and neuromorphic VLSIs.

Tetsuya Asai received the B.S., and M.S., degrees in electrical engineering from Tokai University, Kanagawa, Japan, in 1993 and 1996 respectively, and the Ph.D. in electrical and electronic engineering from Toyohashi University of Technology, Aichi, Japan, in 1999. He is now Associate Professor in the Graduate School of Information Science and Technology, Hokkaido University, Sapporo, Japan. His current research interests include nonlinear analog processing in neural networks and reaction-diffusion systems as well as design and applications of neuromorphic VLSIs.

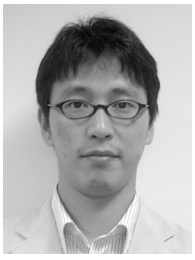

Tetsuya Hirose received the B.S., M.S. and Ph.D. degrees from Osaka University, Osaka, Japan, in 2000, 2002, and 2005, respectively. Currently, he is a Research Associate in the Department of Electrical Engineering, Hokkaido University, Sapporo, Japan. His current research interests are in low-power analog/digital CMOS circuits and subthreshold MOS-FET functional circuits for intelligent sensors. Dr. Hirose is a member of the IEEE.

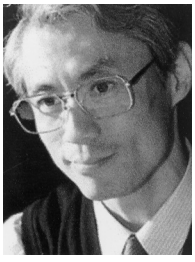

Yoshihito Amemiya received the B.E., M.E., and Dr. Engineering degrees from the Tokyo Institute of Technology, Tokyo, Japan, in 1970, 1972, and 1975. He joined NTT Musashino Laboratories in 1975, where he worked on the development of silicon process technologies for high-speed logic LSIs. From 1983 to 1993, he was with NTT Atsugi Laboratories and developed bipolar and CMOS circuits for Boolean logic LSIs, neural network LSIs, and cellular automaton LSIs. Since 1993, he has been a Professor with the Department of Electrical Engineering, Hokkaido University, Sapporo. His research interests are in the fields of silicon LSI circuits, signal processing devices based on nonlinear analog computation, logic systems consisting of single-electron circuits, and information-processing devices making use of quantum nanostructures.